PHARMACIA

Pharmacia 69(2): 415–428
DOI 10.3897/pharmacia.69.e83158

Research Article

Synthesis, docking study, and structure activity relationship of novel anti-tumor 1, 2, 4 triazole derivatives incorporating 2-(2, 3- dimethyl aminobenzoic acid) moiety

Hiba Alsaad[1], Ammar Kubba[2], Lubna H. Tahtamouni[3,4], Ali H. Hamzah[5]

1 *Department of Pharmaceutical Chemistry, College of Pharmacy, University of Basrah, Basrah, 61001, Iraq*
2 *Department of Pharmaceutical Chemistry, College of Pharmacy- Bab-Almoudam, University of Baghdad,Baghdad-Iraq*
3 *Department of Biology and Biotechnology, Faculty of Science, The Hashemite University, Zarqa, Jordan*
4 *DDepartment of Biochemistry and Molecular Biology, College of Natural Sciences, Colorado State University, Fort Collins, Colorado, USA*
5 *Department of Medicinal and Biological Chemistry, University of Toledo, Toledo, Ohio, USA*

Corresponding author: Hiba Alsaad (hiba.jassem@uobasrah.edu.iq)

Received 6 March 2022 ♦ **Accepted** 14 April 2022 ♦ **Published** 11 May 2022

Citation: Alsaad H, Kubba A, Tahtamouni LH, Hamzah AH (2022) Synthesis, docking study, and structure activity relationship of novel anti-tumor 1, 2, 4 triazole derivatives incorporating 2-(2, 3- dimethyl aminobenzoic acid) moiety. Pharmacia 69(2): 415–428. https://doi.org/10.3897/pharmacia.69.e83158

Abstract

A series of 1,2,4 triazole derivatives (H7-12) have been synthesized by reacting an excess of hydrazine hydrate with carbothioamide derivatives (H1-6). The final compounds (HB1-HB6) were synthesized by reacting the triazole derivatives with mefenamic acid using DCC as a coupling agent. The chemical structures were confirmed by FT-IR, ^{1}H, and ^{13}C-NMR spectra, and some physicochemical properties were determined. The cytotoxicity of the different compounds (HB1-HB6) was evaluated by the MTT assay against two human epithelial cancer cell lines, A549 lung carcinoma and Hep G2 hepatocyte carcinoma, and one normal human cell line WI-38 lung fibroblasts. The mode of cell killing (apoptosis versus necrosis), as well as the effect on cell cycle phases were evaluated via flow cytometry. Additionally, EGFR tyrosine kinase inhibition assay was performed. The results presented in the current study indicate that the six tested compounds exhibited cytotoxicity against both cancer cell lines, and the lowest IC_{50} was achieved with compound HB5 against Hep G2 cancer cells which was found to be highly selective against cancer cells. HB5-treated Hep G2 cells were arrested at the S and G2/M cell cycle phases. Compound HB5 caused cell killing via apoptosis rather than necrosis, and this was achieved by inhibiting EGFR tyrosine kinase activity needed for cell proliferation, and cell cycle progression. In silico *pre*-ADMET studies confirmed all final compounds don't cause CNS side effects, with little liver dysfunction effect.

Keywords

1,2,4 triazole, MTT assay, apoptosis, EGFR tyrosine kinase activity, *pre*-ADMET

Introduction

Cancer is one of the major global health burdens representing the second major cause of death worldwide (WHO 2020). Cancer is an intricate series of disease states that involves losing control of regular cell growth. For decades, the known protocols for cancer treatment have been either the use of single or combination therapeutics

which include chemotherapy, surgery, and radiation therapy (Debela et al. 2021). Today, several studies have been focusing on developing new therapies with limited side effects as compared to conventional medications (Iacopetta et al. 2020).

Epidermal growth factor has a role in cell growth stimulation and differentiation through binding to its receptor, the epidermal growth factor receptor (EGFR). EGFR is a transmembrane protein belonging to the ErbB family of receptors. The ErbB is a subfamily of tyrosine kinase receptors including EGFR (ErbB-1), HER2/neu (ErbB-2), HER3 (ErbB-3), and HER4 (ErbB-4). EGFR is often upregulated in several cancers such as breast cancer, non-small-cell lung cancer (NSCLC), hepatocellular carcinoma (HCC), and glioblastoma (Sigismund, Avanzato and Lanzetti 2018a; Arienti et al. 2019; Maennling et al. 2019; Liu et al. 2021). The binding of EGF to the extracellular domain of EGFR causes homodimerization or heterodimerization of ErbB family receptors, which results in phosphorylation of intracellular Tyr1173 and Tyr1068 residues of EGFR. This in turn initiates several signaling pathways such as, phosphoinositide-3-kinase (PI3K)/serine/threonine-specific protein kinase (Akt), RAS/mitogen-activated protein kinase (MAPK), and Janus kinase/signal transducer and stimulation of transcription (Jak/Stat) pathways. The activation of these pathways mediates cellular proliferation and transformation, which in turn may cause invasion, growth, and cancer metastasis (Gurdal et al. 2019; Belli et al. 2020).

Heterocyclic compounds are interesting structures for medicinal chemists due to their important chemical and biological properties. Although many heterocyclic compounds have been developed, efforts are still ongoing to produce a new heterocyclic ring system with important biological activity (Al-Bayati et al. 2021a). One interesting heterocyclic compound is triazole, which consists of a five-member ring with 3N atoms and the chemical formula $C_2H_3N_3$. 1,2,4 triazole nucleus has the greater benefit for researchers because of its extended applications in pharmaceutical, agrochemical, and material sciences (Kaur et al. 2016). The 1, 2, 4-triazole rings are stable against metabolic degradations and show target selectivity as well as several pharmacological activities. The nitrogen atoms in the triazole moiety play an important role in binding the receptor by forming bonds via H-bond donors or acceptors (Chopra et al. 2018; Kerru et al. 2020; Al-Bayati et al. 2021b). Significant improvement in both pharmacokinetics and pharmacodynamics of ligand-containing triazole rings is expected due to a rise in water solubility owing to the polar characteristics (Al-Bayati et al. 2021b). Many studies have shown that this important pharmacophore nucleus has important role in different types of anti-cancer compounds such as kinase inhibitors, tankyrase inhibitors, methionine aminopeptidase inhibitors, tubulin modulators, aromatase, nucleoside-based anticancer agents, steroid sulfatase inhibitors, and metal complex based anti-cancer agents (Zhang et al. 2020).

The ability of 1,2,4 triazole derivatives to form different types of non-covalent interactions such as hydrogen bonds, van der Waals forces, hydrophobic interactions, and dipole-dipole bonds with various biological targets, is responsible for diverse therapeutics properties including their antibacterial (Grytsai et al. 2020), antimalarial (Chu et al. 2019), antifungal (Peyton et al. 2015), antiviral (El-Sebaey 2020), antitubercular (Shaikh et al. 2019), and anticancer activities (Lakkakula et al. 2019; Krishna et al. 2020). Furthermore, compounds that have triazole moiety could display antioxidant activity either through inhibition of lipid peroxidation or scavenging activity for ROS (reactive oxygen species) (Das et al. 2019).

Additionally, one of the important medications based on triazole nucleus which possess anti-proliferative activity against different types of cancer are the non-steroidal anti-inflammatory drugs (NSAIDs) (Kuntala et al. 2021). Their ability to inhibit cyclooxygenase-2 (COX-2) was proposed to be a mediator for their anti-tumor activity, but higher doses were required. Moreover, studies have indicated that NSAIDs induce apoptosis in many types of cancer cell lines such as colon, stomach, and prostate (Woo et al. 2004; Kazberuk et al. 2020).

In this regard, the objective of this study was to design and synthesize some novel 1, 2, 4-triazole derivatives incorporating 2-(2, 3- dimethyl aminobenzoic acid) moiety. Different electron withdrawal and donating groups at the *p*-position of benzene moieties were chosen to improve the physicochemical properties and cytotoxicity of the new synthetic compounds.

Experimental part

Material and methods

The chemical reagents and solvents were used without further purification from Sigma-Aldrich, Milano, Italy and Merck, Taufirchen, Germany. Mefenamic acid was purchased from Pioneer Company (Erbil, Iraq). Infrared spectra were measured using a Shimadzu model 8400s (Nakagyo, Japan) spectrophotometer on disk of KBr, ($v = cm^{-1}$). Elemental microanalysis (CHNS) was done using a Euro EA300 elemental analyzer (Carlo Erba, Emmendingen, Germany). The proton (^1H) and carbon (^{13}C) NMR spectra were measured using the Inova model Ultra shield at 500, and 125 MHz respectively, δ= ppm was used to express the chemical shift. The solvent used was $DMSO_{d6}$.

Chemical synthesis

The intermediates and final compounds were synthesized according to Scheme 1.

Synthesis of methyl ester derivatives: compounds (3 and 4)

Few drops of conc. H_2SO_4 were added to 10 mmol of benzoic acid (1) or *p*-nitro benzoic acid (2) in 30 mL MeOH, the mixture was then refluxed for 3h. The product was

formed after neutralization of the reaction mixture with Na_2CO_3. Compound (3) was obtained by extracting the aqueous layer with chloroform, and dried using anhyd. $MgSO_4$. While compound (4) was filtrated after precipitation and recrystallized with EtOH. The physical properties are mentioned in Table 1.

Methyl benzoate (3): FT-IR(v = cm^{-1}): 1724 (C=O) of ester.

Methyl 4-nitrobenzoate (4): FT-IR: 1731(v = cm^{-1}): (C=O) of ester.

Synthesis of aryl hydrazide derivatives: compounds (5 and 6)

To 10 mmol of compound (3) or (4) in 15mL EtOH, 30 mmol of hydrazine hydrate was added. The mixture was refluxed for 4h, the solvent was then reduced using a rotary evaporator, and the residual was added to ice water. The formed precipitate was filtered, and recrystallized from EtOH (Shabeeb et al. 2019). The physical properties are mentioned in Table 1.

N-(aminomethyl) benzamide (5): FT-IR(v=cm^{-1}) :3501.11 and 3456.81 (-NH) str. of NH_2; 3344.47 (-NH) str. of (CONH); 1660 (C=O) str. of amide.

N-(aminomethyl)-4-nitrobenzamide (6): FT-IR(v=cm^{-1}): 3380.66 and 3290.27 (-NH) str. ofNH_2; 3130.69 (-NH) str. of (CONH); 1683.2 (C=O) str. of amide.

Synthesis of carbothioamide derivatives compounds (H 1-6)

To 5 mmol of compound (5) or (6) in 10 mL MeOH, 5 mmol of different aryl isothiocyanate derivatives in 5 mL MeOH was added. The reaction was stirred under 50 °C for 1h. The precipitate was filtered and washed with hot MeOH (Al-Saad et al. 2019). The physical properties are mentioned in Table 1.

Table 1. Physical properties of the intermediates and final compounds.

Compound	Appearance	Yield %	M.p.\ b.p °C	*R_f
3	Oily liquid	90	199	0.8
4	Pale- yellow	92	94-95	0.83
5	White crystal	85	120-121	0.49
6	Yellow crystal	88	142-143	0.41
H1	White powder	78	148-149	0.35
H2	White powder	79	166-168	0.36
H3	White powder	84	160-161	0.33
H4	Yellow powder	72	168-169	0.33
H5	Yellow powder	80	180-181	0.32
H6	Yellow powder	75	175-177	0.34
H7	Red powder	62	160-161	0.54
H8	Brown powder	50	178-179	0.56
H9	Orange powder	70	185-186	0.53
H10	Brown powder	63	190-191	0.6
H11	Brown powder	64	202-203	0.62
H12	Orange powder	67	193-194	0.61
HB1	Dark-orange powder	47	206-207	0.83
HB2	Dark-brown powder	52	211-212	0.85
HB3	Brown powder	48	218-219	0.83
HB4	Brown powder	56	220-221	0.92
HB5	Dark-red powder	50	230-231	0.95
HB6	Dark-brown powder	43	225-226	0.94

* Eluent: n-hexane: ethyl acetate (1:1).

2-benzoyl-N-phenylhydrazine-1-carbothioamide (H1): FT-IR(v=cm^{-1}): 3233.16 *br.* (-NH) str. of (CONHNHCSNH); 3171.65 str. of (Ar-CH).; 1690.11 str. of (C=O) amide; 1566.82, 1507.22 and 1450.69 str of (Ar-C=C); 1189.5 str. of (C=S)

2-benzoyl-N-(4-chlorophenyl)hydrazine-1-carbothioamide (H2): FT-IR(v=cm^{-1}): 3262.91 *br.* (-NH) str. of (CONHNHCSNH); 1683.56 str. of (C=O) amide; 1181.14 str. of (C=S); 1088.46 str. of (C-Cl).

2-benzoyl-N-(4-methoxyphenyl)hydrazine-1-carbothioamide (H3): FT-IR(v=cm^{-1}): 3263.81 *br*. str. (-NH) of (CONHNHCSNH); 3144.91 str. of (Ar -CH); 1679.98 (C=O) str. of amide; 1542.25, 1522.5 and 1452.11 str. of (Ar-C=C); 1244 *asym* str. of (C-O); 1182.55 str. of (C=S); 1027 *sym* str. of (C-O).

2-(4-nitrobenzoyl)-N-phenylhydrazine-1-carbothioamide (H4): FT-IR((v=cm^{-1}): 3237.2 *br*. str. (-NH) of (CONHNHCSNH); 1686.31(C=O) str. of amide; 1546.22, 1511.24 and 1453.61 str. of (Ar-C=C); 1182.3 str. of (C=S).

N-(4-chlorophenyl)-2-(4-nitrobenzoyl)hydrazine-1-carbothioamide(H5): FT-IR(v=cm^{-1}): 3265.33 *br.* str. (-NH) of (CONHNHCSNH); 1690.76 (C=O) str. of amide; 1177.42 str. of (C=S); 1087.56 str. of (C-Cl).

*N-(4-methoxyphenyl)-2-(4-nitrobenzoyl)hydrazine-1-carbothioamide(H6):*FT-IR (v=cm^{-1}): 3271.55 *br.* str. (-NH) of (CONHNHCSNH); 1684.58 (C=O) str. of amide; 1566.35; 1511.64 and 1455.17 Ar(C=C) str.; 1245.22 *asym* str. of (C-O); 1185.55 str. of (C=S); 1029 *sym* str. of (C-O).

Synthesis of 1,2,4 triazole derivatives, compounds (H 7-12)

2 mmol of compounds (H1-6) was suspended in 10 mL of MeOH, and 10 mmol of hydrazine hydrate was added. A red mixture was formed and refluxed for 20h. The solvent was reduced with a rotary evaporator. 5 mL of Et_2O were added to the residual and kept for 24h at a cold place. The precipitate was washed repeatedly with diethyl ether, and dried overnight at 25 °C (Fattah 2014). The physical properties are mentioned in Table 1.

N^3,5- diphenyl-4H-1,2,4- triazole-3,4- diamine (H7): FT-IR(v=cm^{-1}): 3390.11 and 3340.01 (NH) str. of 1° amine; 3329.61 str. of (-NH) of *sec*. amine; 1680.58 (C=N) str. of imine.

N^3- (4-chlorophenyl)-5-phenyl-4H-1,2,4- triazole-3,4-diamine (H8): FT-IR(v=cm^{-1}): 3385.78 and 3347.13 str. (NH) of 1° amine; 3325.62 str. (-NH) of *sec*. amine; 1685.35 (C=N) str.of imine.

N^3- (4-methoxyphenyl)-5-phenyl-4H-1,2,4- triazole-3,4-diamine (H9): FT-IR(v=cm^{-1}): 3400 and 3359.2 str. (NH) of 1° amine; 3333.53 str. (NH) of *sec*. amine; 1688.34 (C=N) str. of imine.

5- (4-nitrophenyl)-N3-phenyl-4H-1,2,4- triazole-3,4-diamine (H10): FT-IR(v=cm^{-1}): 3393.45 and 3352.9 str. (NH) of 1° amine; 3311.71 str. (NH) of *sec*. amine; 1672.71 (C=N) str. of imine; 1542.16 (N-O) *asym* str. of NO_2, 1376 (N-O) *sym* str. of (NO_2).

N^3- (4-chlorophenyl)-5-(4-nitrophenyl)-4H-1,2,4- triazole-3,4-diamine (H11): FT-IR(v=cm^{-1}): 3420.23 and 3372

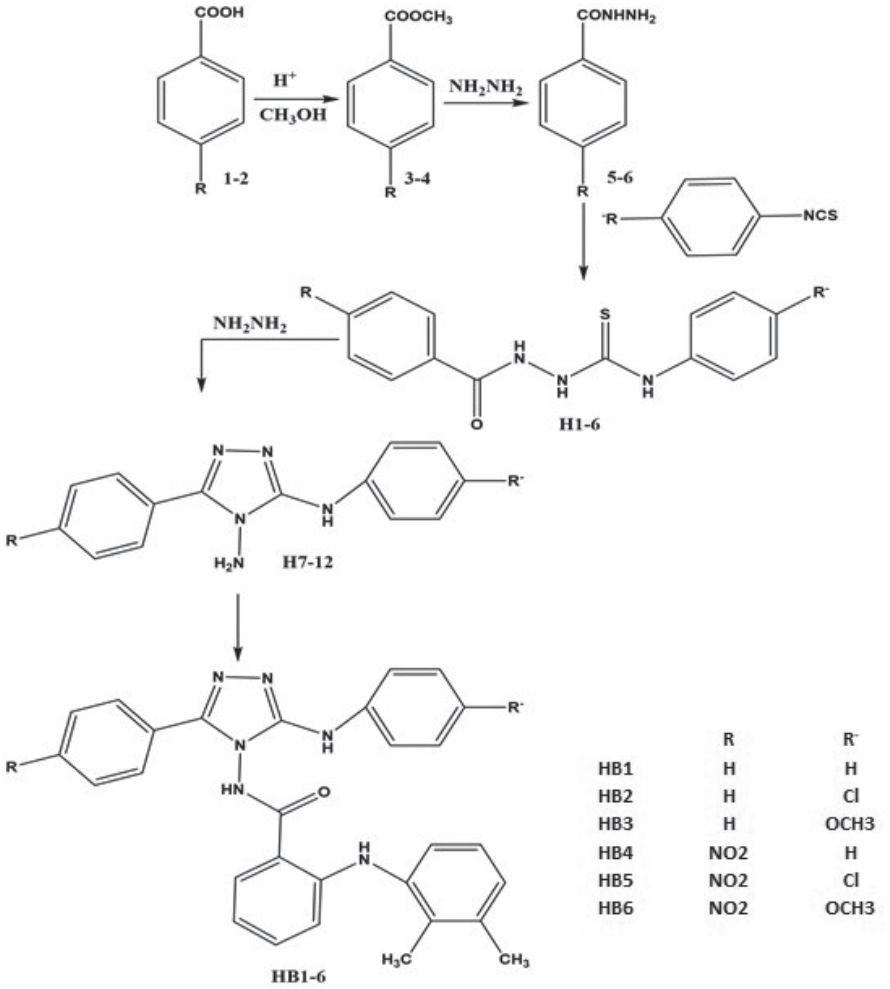

Scheme 1. Chemical synthesis of target compounds (HB1-6).

str. (NH) of 1° amine; 3304.15 str. (NH) of *sec*. amine; 1690.21 (C=N) str. of imine; 1542.61 (N-O) *asym* str. of NO_2, 1379 (N-O) *sym* str. of (NO_2).

N^3- (4-methoxyphenyl)-5-(4-nitrophenyl)-4H-1,2,4-triazole-3,4-diamine (H12): FT-IR(v=cm^{-1}): 3411 and 3362 str. (NH) of 1° amine; 3332.65 str. (NH) of *sec*. amine; 1683.71 str. (C=N) of imine; 1543.11 (N-O) *asym* str. of NO_2, 1380 (N-O) *sym* str. of (NO_2).

Synthesis of amide derivatives (compounds HB 1-6)

10 mmol of mefenamic acid was dissolved in (5mL dioxan and 10 mL THF) on ice bath, to this solution, 10 mmol of DMAP, and 10 mmol of the corresponding compounds (H7-12) were added, respectively. 10 mmol of N, N^-- dicyclohexylcarbodiimide (DCC) in 5 mL of dichloromethane CH_2Cl_2 was added. The mixture was stirred at 0 °C for 3 days. The product was filtered to remove DCU, and the solvent was reduced using a rotary evaporator. EtOAc (5mL) was added to the residual, and the mixture was washed with 10% HCl, 5%$NaHCO_3$, and H_2O, respectively. The organic layer was dried with anhyd. $MgSO_4$, and left to dry for 24h (Mahdi and Alsaad 2012). The physical properties are mentioned in Table 1.

2-((2,3-dimethylphenyl)amino)-N-(3-phenyl-5-(phenylamino)-4H-1,2,4-triazol-4-yl)benzamide (HB1): FT-IR(v=cm^{-1}): 3303.3 (NH) str; 1680.4 (C=O) str, 1665 (C=N). ^{1} HNMR(500MHz,$DMSO_{d6}$,δ=ppm) : 2.1 (s, 3H, CH_3), 2.3 (s, 3H, CH_3), 3.7(s, 2H, *aliph*. NH), 6.0–8.2 (m, 17H, Ar.CH), 8.5 (s, 1H, NH-C=O). ^{13}C-NMR(125MHz,$DMSO_{d6}$,δ=ppm); 18.9 and 20.2 $C_{(methyl)}$; 115.4, 118.2, 118.8, 121.3, 125.5, 126.1, 126.9, 127.3, 127.7, 128.5, 129.0, 129.4, 130.0, 131.4, 132.6, 133.5, 138.2, 138.8, 139.3, 145.2,$C_{(Aromatic)}$, 155.03 and 157 $C_{(Traiazole)}$, 180 $C_{(carbonyl)}$. CHN analysis: Calcd, for ($C_{29}H_{26}N_6O$), MW: 473.22, C: 73.40; H: 5.52; N: 17.71. Observed C: 73.37; H: 5.53; N: 17.70.

N-(3-((4-chlorophenyl)amino)-5-phenyl-4H-1,2,4-triazol-4-yl)-2-((2,3-dimethylphenyl)amino)benzamide (HB2): FT-IR(v=cm^{-1}): 3320.81 (N-H) str; 1681.61 (C=O) str; 1660.23 (C=N) str. ^{1}HNMR(500MHz,$DMSO_{d6}$,δ=ppm): (2.4 (s, 3H, CH_3), 2.7 (s, 3H, CH_3), 4.2(s, 2H, *aliph*. NH), 6.4–7.9(m, 16H, Ar. CH), 8.8 (s, 1H, NH-C=O). ^{13}C-NMR(125MHz,$DMSO_{d6}$,δ=ppm): 19.2 and 20.3 $C_{(methyl)}$, 115.4, 118.1, 118.8, 121.3, 125.5, 126.3, 126.8, 127.3, 127.7, 128.1, 128.7, 129.0, 130.0, 131.3, 132.5, 133.5, 138.2, 138.8, 139.3, 145.2 $C_{(Aromatic)}$, 155.2 and 156.9 $C_{(Traiazole)}$, 181.2 $C_{(carbonyl)}$. CHN analysis: Calcd. for ($C_{29}H_{25}ClN_6O$): MW: 509.01, C: 68.43; H: 4.95; Cl: 6.96; N: 16.51. Observed: C: 68.44; H: 4.93; CI: 6.98; N: 16.52.

2-((2,3-dimethylphenyl)amino)-N-(3-((4-methoxyphenyl) amino)-5-phenyl-4H-1,2,4-triazol-4-yl)benzamide (HB3): FT-IR(v=cm^{-1}): 3326.62 (NH), 2874.99, and 2825.51 (C-H) *aliph.* str, 1688.22 (C=O); 1654.65 (C=N). ^{1}HNMR 500MHz, $DMSO_{d6}$, δ=ppm): 2.3 (s, 3H, CH_3), 2.7 (s, 3H, CH_3), 3.5(s, 3H, -OCH_3), 4.1(s, 2H, *aliph.* NH), 6.5–8.2(m, 16H, Ar. CH), 8.4 (s, 1H, NH-C=O). ^{13}CNMR(125MHz,$DMSO_{d6}$,δ=ppm): 19.2 and 20.3 $C_{(methyl)}$; 62.9 $C_{(methoxy)}$ 115.1, 115.8, 118.1, 118.7, 120.3, 121.3, 126.1, 126.9, 127.3, 128.5, 129.0, 129.6, 130.1, 131.4, 132.6, 133.7, 138.1, 138.8, 139.3, 145.2 $C_{(Aromatic)}$;152.5 and 157.1 $C_{(Traiazole)}$,181.2 $C_{(carbonyl)}$. Elemental analysis: Calcd. for ($C_{30}H_{28}N_6O_2$): MW: 504.59, C: 71.41; H: 5.59; N: 16.66. Observed C: 71.4; H: 5.58; N: 16.68.

2-((2,3-dimethylphenyl)amino)-N-(3-(4-nitrophenyl)-5-(phenylamino)-4H-1,2,4-triazol-4-yl)benzamide(HB4): FT-IR(v=cm^{-1}): 3301.54 (NH); 2860.05, and 2843.12 (C-H) *aliph.* str, 1669.88 (C=O), 1645.76 (C=N). ^{1}HNMR(500MHz,DMSO*d6*,δ=ppm): 2.0 (s, 3H, CH_3), 2.2 (s, 3H, CH_3), 4.1(s, 2H, *aliph.* NH), 6.9–8.5(m, 16H, Ar. CH), 8.3 (s, 1H, NH-C=O). ^{13}CNMR(125MHz,$DMSO_{d6}$,δ=ppm): 19.3 and 20.4 $C_{(methyl)}$; 114.2, 118.2, 118.7, 121.9, 124.8, 126.1, 126.7, 127.4, 127.6, 128.5, 129.0, 129.7, 131.4, 132.5, 133.6, 138.2, 138.8, 139.5, 145.7, 149.3$C_{(Aromatic)}$; 152.0 and 157.0 $C_{(Traiazole)}$, 182.0 $C_{(carbonyl)}$. Elemental analysis: Calcd. for ($C_{29}H_{25}N_7O_3$): MW: 519.57, C: 67.04; H: 4.85; N: 18.87. Observed: C: 67.01; H: 4.85; N:18.89.

N-(3-((4-chlorophenyl)amino)-5-(4-nitrophenyl)-4H-1,2,4-triazol-4-yl)-2-((2,3-dimethylphenyl)amino) benzamide (HB5): FT-IR(v=cm^{-1}): 3301.99 (NH); 2889.27, and 2853.45 (C-H) *aliph.* str 1686.2 (C=O) str, 1666.3 (C=N). ^{1}HNMR: 2.0 (s, 3H,CH_3), 2.5 (s, 3H, CH_3), 3.5(s, 2H, *aliph.* NH), 6.6–8.8(m, 15H, Ar-CH), 8.7 (s, 1H, NH-C=O). ^{13}CNMR(125MHz,$DMSO_{d6}$,δ=ppm): 19.2 and 20.21 $C_{(methyl)}$, 114.3, 118.2, 118.9, 121.6, 125.8, 126.1, 126.8, 127.4, 127.9, 128.4, 129.3, 129.9, 131.3, 132.4, 133.5, 133.9, 138.8, 139.7, 146.3, 149.5 $C_{(Aromatic)}$; 152.0 and 155.0 $C_{(Traiazole)}$, 183.0 $C_{(carbonyl)}$. Elemental analysis: calcd. for ($C_{29}H_{24}ClN_7O_3$): MW: 554.01, C: 62.87; H: 4.37; Cl: 6.40; N: 17.70. Observed: C: 62.87; H: 4.34; CI: 6.42; N: 17.68.

2-((2,3-dimethylphenyl)amino)-N-(3-((4-methoxyphenyl) amino)-5-(4-nitrophenyl)-4H-1,2,4-triazol-4-yl)benzamide (HB6): FT-IR(v=cm^{-1}): 3300.72 (NH) str, 1683.22 (C=O) str, 1660.1 (C=N) str. ^{1}HNMR(500MHz,DMSO*d6*,δ=ppm): 2.3 (s, 3H, CH_3), 2.4 (s, 3H, CH_3), 3.5 (s, 3H, OCH_3), 4.2(s, 2H, *aliph.* NH), 6.2–8.9(m, 15H, Ar-CH), 8.5 (s, 1H, NH-C=O). ^{13}CNMR; 18.4 and 20.5 $C_{(methyl)}$; 61.4 C $_{(methoxy)}$; 115.3, 115.9, 118.1, 119.0, 120.2, 121.6,125.5, 126.1, 126.9, 127.7, 128.3, 129.1, 129.8, 131.3, 132.5, 133.6, 138.3, 139.8, 145.8, 149.5 $C_{(Aromatic)}$, 152 and 157 $C_{(Traiazole)}$, 181.9 $C_{(carbony)}$. Elemental analysis: calcd. for ($C_{30}H_{27}N_7O_4$): MW: 549.59, C: 65.56; H: 4.95; N: 17.84. Observed C: 65.55; H: 4.99; N: 17.84.

Docking study

The chemical structure of the designed compounds was compared with crystal ligands to choose the molecular targets. A protein data bank (PDB) (https://www.rcsb.org/) was used to select the target site, additionally, the main requirements for binding with essential amino acids in the target site were determined.

Method of the docking study

Molecular Operating Environment 19.0901 software was used to predict the binding modes of the designed compounds inside target sites of EGFR tyrosine kinase. The ligand-binding sites were created from a co-crystallized structure within PDB (ID: 1M17) (https://www.rcsb.org).

Initially, water molecules were reduced from the complex. The clean protein options and protein report and utility were used to correct unfilled valence atoms and crystallographic disorders. The protein energy was reduced using MMFF94 force fields, while fixed atom constraint was applied to obtain the protein rigid binding site. 2D structures were generated using ChemBioDraw Ultra16.0 and saved in MDL-SD form. The 3D structures were protonated after opening in MOE, 0.05 RMSD kcal/mol was applied to minimize the energy, and the docking protocol was used for docking the minimized structures. CDOCKER protocol was used to accomplish the process of molecular docking. The ligands were permitted to be flexible while the receptor was held rigid. Thirty conformation poses were used in the placement process, scored by London ΔG, and the best 10 docking scores (ΔG) of fitted poses with the active site at EGFR tyrosine kinase (scored by GBVI/WSA) were used and 3D perspective was done by Discovery Studio 2019 Client software.

These methods were also used to anticipate the binding profile, ideal orientation of each docking pose, affinity, and binding free energy (ΔG) of the prepared compounds with EGFR tyrosine kinase.

In silico ADMET and drug-likeness prediction

In-silico study ADMET along with drug-likeness prediction assist the drug discovery and development process. Here, *Pre*-ADME online software was utilized for estimating absorption, distribution, metabolism, excretion, and toxicity (ADMET) profiling of the tested compounds. These descriptors involve human gastrointestinal absorption, bioavailability, penetration to the blood-brain barrier, binding to plasma protein, inhibition of liver enzymes, and carcinogenesis. The drug-likeness of the derivatives were predicted following Lipinski's Rule. The measured parameters were number of H-bond donors and acceptors, clog p, and Topological Polar Surface Area (TPSA). The study was done using Chem. Informatics on the web (http://www.molinspiration.com).

Biological study

Cell culture

Human A549 lung cancer cell line was grown in Ham's F-12K medium (Thermo Scientific, USA) supplemented with fetal bovine serum (10%) (FBS; Gibco, USA), human Hep G2 hepatocyte carcinoma cell line and human WI-38 cell line (lung fibroblasts) were grown in Eagle's minimum

essential medium (LONZA, Switzerland), to which 10% FBS was added. Trypsin-EDTA (Millipore-Merck, USA) was used during subcultures. Growth of cells was established at 37 °C in 5% CO_2 and 95% air.

In vitro MTT cell proliferation assay

The MTT assay was used to evaluate the proliferation of control and treated cells (Mosmann 1983). 96-well plates were used throughout the experiment. 30,000 cells were added to each well containing the appropriate media and grown for 24 h. The stock solutions of each of the tested compounds were prepared in DMSO. Eight concentrations (100, 30, 10, 3, 1, 0.3, 0.1, and 0.03 µM) were prepared in the growth media for each compound and added to the cells for 48 h. MTT salt (Freshly prepared; 3-(4,5-dimethylthiazol-2yl)-2,5- diphenyltetrazolium bromide) (5 mg/ml; Sigma) was then added to each well to obtain 0.5 µg/µL as a final concentration. 200 µL of DMSO and isopropanol mixture 1:1 was added to each well and incubated for 30–45 min. Cell proliferation was detected by measuring the absorbance of each well at 590 nm using Multiskan EX (Thermo Scientific, USA) MicroPlate Reader. The experiment was performed three times in triplicates.

Table 2. The sequence of qRT-PCR primers, forward (F) and reverse (R), used in the current study.

Gene	Primer sequence	Reference
p53	F: 5'- GCCCAACAACACCAGCTCCT -3'	(Zhang et al. 2019)
	R: 5'-CCTGGGCATCCTTGAGTTCC -3'	
BAX	F: 5'- CCCGAGAGGTCTTTTTCCGAG -3'	(Jiang et al. 2020)
	R: 5'- CCAGCCCATGATGGTTCTGAT -3'	
Bcl-2	F: 5'- TTGTGGCCTTCTTTGAGTTCGGTG -3'	(Khodapasand et al. 2015)
	R: 5'- GGTGCCGGTTCAGGTACTCAGTCA -3'	
Caspase-3	F: 5'- ACATGGAAGCGAATCAATGGACTC -3'	(Peluffo, Young and Stouffer 2005)
	R: 5'- AAGGACTCAAATTCTGTTGCCACC -3'	
GAPDH	F: 5'- GACCCCTTCAT GACCTCAAC -3'	
	R: 5'- CTTCTCCATGGTGGT GAAGA -3'	

Table 3. The energy of binding (ΔG) kcal/mol of the candidate compounds (HB1-HB6) against EGFR tyrosine kinase target site PDB ID: 1M17.

Ligand	RMSD value (Å)	Docking score(ΔG) (kcal/mol)	Interactions	
			H-bond	pi
Compound HB1	1.85	-7.08	–	7
Compound HB2	1.90	-7.47	1	8
Compound HB3	1.98	-7.50	–	6
Compound HB4	1.45	-7.82	1	6
Compound HB5	1.74	-8.32	1	7
Compound HB6	1.99	-7.15	1	9
Erlotinib	1.90	-6.55	1	6

Cell cycle analysis

Hep G2 cells were treated with the IC_{50} concentration of drug HB5 (2.87 µM) for 48 h (see Table 3). Control and treated cells were trypsinized and the cell suspension was fixed in EtOH solution (70%) at 4 °C for 120 min and then centrifuged at 800× g in a low-temperature centrifuge (Eppendorf, USA) for 5 min. The cell pellet was washed twice with phosphate buffer solution (PBS), centrifuged, and suspended in 0.5 mL PBS containing 20 µg/mL propidium iodide (PI) and 100 µg/mL Ribonuclease A. After incubation for 30 min at 37 °C in the dark, cells were centrifuged, and the cell pellet was suspended in PBS (Cell Cycle Assay Kit; Elabscience Biotechnology, USA). The fluorescence of the PI-DNA complex was detected using Epics XL-MCL Flow Cytometer (Beckman Coulter) and the Flowing software (version 2.5.1, Turku Centre for Biotechnology, Turku, Finland) was used to analyze the cell distribution at different stages of the cell cycle: sub-G1; G1; S; and G2/M (Nunez 2001; Pozarowski and Darzynkiewicz 2004).

Detection of apoptosis/necrosis

Hep G2 cells were treated with the IC_{50} concentration of drug HB5 (2.87 µM) for 48 h. Apoptosis (early and late)/necrosis induction was detected in control and treated cells by phosphatidylserine translocation to the cell surface using annexin V-FITC apoptosis detection kit (Elabscience Biotechnology, USA).

Quantitative reverse transcription-polymerase chain reaction (qRT-PCR)

The quantity of BAX, Bcl-2, p53, and caspase 3 mRNA in control and HB5 (at the IC_{50} concentration)-treated Hep G2 cells were assessed by qRT-PCR. Total RNA from vehicle-treated control (0.01% DMSO) and HB5-treated Hep G2 cells were extracted according to the manufacturer's instructions (RNeasy mini kit, Qiagen, Germany). After RNA extraction, cDNA was prepared using the Revert Aid First Strand cDNA Synthesis kit (Thermo Scientific, USA). Amplification of target cDNA for apoptosis markers and GAPDH [as a normalization (housekeeping) gene] was done using one-step RT-PCR SYBR Green kit Master Mix (Bio-Rad Laboratories, USA) on Rotor-Gene Q real-time PCR thermal cycler instrument. cDNA (2 µL aliquots) was mixed with forward primer (1 µL), reverse primer (1 µL) (Table 2), master mixture (10 µL) and the reaction volume was completed to (20 µL) with nuclease-free water. All experiments were performed in triplicate.

Epidermal growth factor receptor (EGFR) tyrosine kinase inhibitory assay

The *in*-vitro inhibitory activity of compound HB5 and erlotinib [standard receptor-tyrosine kinase inhibitor (TKI)] against EGFR tyrosine kinase was done using EGFR Kinase Assay Kit (BPS Bioscience, USA). Briefly, EGFR and its substrate were incubated either with HB5 or erlotinib (1000, 300, 100, 30, 10, 3, 1, and 0.3 nM) in the enzymatic buffer at 30 °C for 40 min to initiate the enzymatic reaction. Detection reagent (Kinase-Glo MAX; Promega, USA) was added to terminate the reaction, followed by incubation for 15 min at 25 °C. The

remaining activity of EGFR tyrosine kinase was observed by measuring chemiluminescence using BioTek Synergy2 Microplate Reader (BioTek, USA). The concentration-percent remaining EGFR tyrosine kinase activity curve was used to calculate the concentration that caused 50% kinase activity inhibition (the effective concentration that inhibits 50% of EGFR kinase activity; EC_{50}). All samples and controls were verified in triplicate.

Statistical analysis

Results are recorded as mean ± SEM. GraphPad Prism version 8.0 (GraphPad Software, San Diego, CA, USA) was used for statistical analysis. The student's t-test was used to determine significance between means, p-value < 0.05 was considered significant.

Results and discussion

Docking study

The binding form of the reference (Erlotinib) displayed an energy binding of -6.55 kcal/ mol against EGFR tyrosine kinase. The quinazoline ring formed *pi*-Alkyl interactions with amino acids Val702, Leu694, Leu820, Ala719, and one H-bonding with Met769 with a distance of 2.66 °A. The 3-ethynyl phenyl moiety interacted with Lys721 and Leu764 by *pi*-alkyl interactions as shown in Fig. 1.

The energy of binding (ΔG) of the tested compounds (HB1-6), the number of H-bonds, and *pi* interactions are displayed in Table 3. The 2D docking of compounds (HB1-6) against EGFR tyrosine kinase is shown in Fig. 2, where H-bonds are represented in green lines and the *pi* interactions are represented in purple, orange, and pink lines. Additionally, each of the compounds (HB1-6) were superimposed with erlotinib and both were docked inside the target site of EGFR tyrosine kinase (Fig. 2). The superimposition shows that the fittest compounds were compound HB4 and HB5.

The 4*H*-1,2,4-triazole ring of compound HB1 generated *pi* interactions with the essential amino acids Leu820, Ala719, and Val702 of EGFR tyrosine kinase, while the phenyl moiety formed other *pi* interactions with Ala719, Lys721, and Val702, and the phenylamino moiety formed *pi* interaction with leu694. The binding features of compound HB2 to EGFR tyrosine kinase was through 4*H*-1,2,4-triazole ring which showed *pi* interactions with the essential amino acids Leu820, Ala719, and Val702 of EGFR tyrosine kinase, while the phenyl moiety formed another sulfur-*pi* interaction with Met742, and *pi*-alkyl interaction with Lys721. The 4-chloro phenylamino moiety formed *pi* interaction with Leu694, and the (2,3-dimethyl phenyl) amino moiety formed one H-bond with Asp831 (2.45 °A), and *pi-pi* interaction with Phe699, while the benzamide moiety interacted with Cys773 by sulfur-*pi* interaction.

The 4*H*-1, 2, 4-triazole ring of HB3 formed *pi* interactions with Val702, while the phenyl moiety formed another sulfur-*pi* interaction with Cys773, and the 4-methoxy phenylamino moiety formed *pi* interactions with Lys721, Ala719, and Val702. In addition, the benzamide moiety interacted with Leu694 by *pi*-alkyl interaction.

Compound HB4 interacted with different essential amino acids of EGFR tyrosine kinase: the 4*H*-1,2,4-triazole ring created *pi* interactions with Leu820, Ala719, and

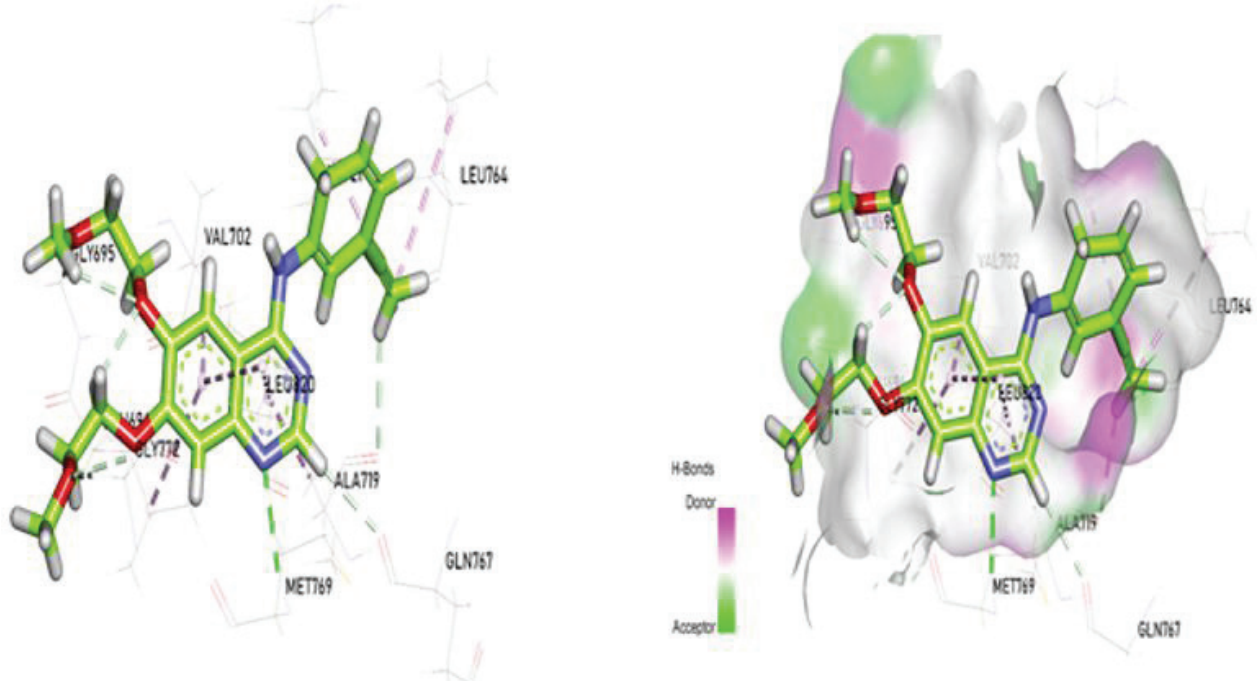

Figure 1. Erlotinib docked on EGFR tyrosine kinase. H-bonds (green) and *pi* interactions (purple lines) with the mapping surface showing erlotinib occupying the active pocket of EGFR tyrosine kinase.

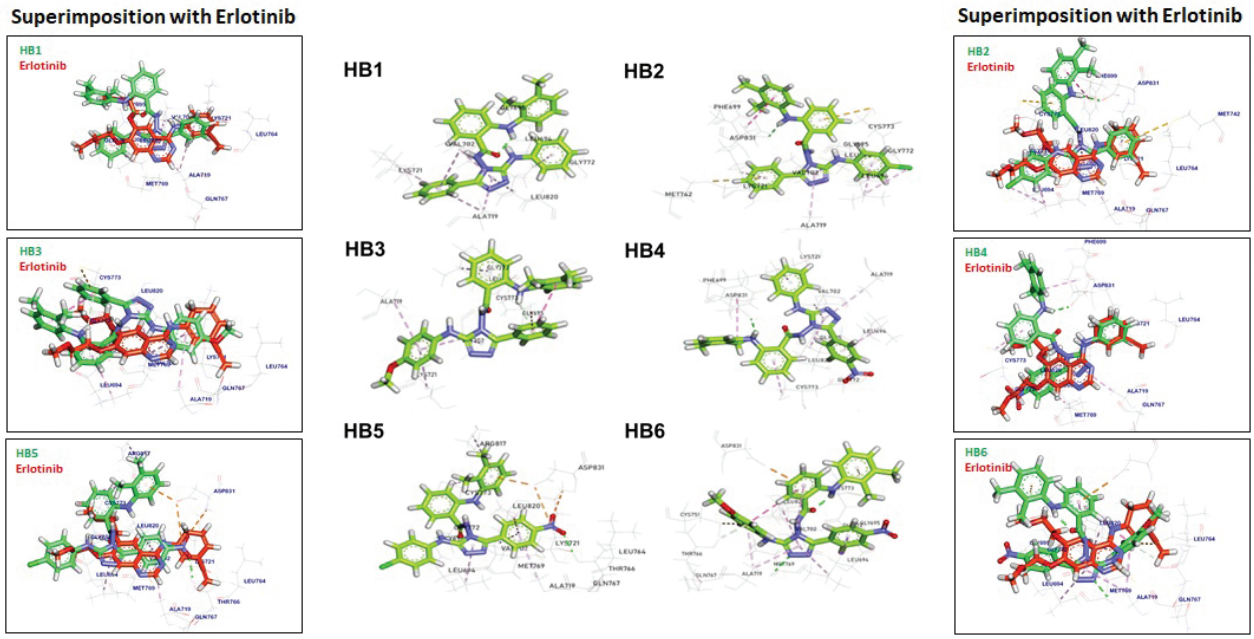

Figure 2. The 2D docking of compounds (HB1-6) against EGFR tyrosine kinase focusing on the interacting amino acids. H-bonds are shown in green dashed lines, and the *pi* interactions are shown in purple, orange, and pink dashed lines. Superimposition of each compound with erlotinib inside EGFR tyrosine kinase target site is shown.

Val702, while the phenylamino moiety formed *pi* interaction with Lys721. The 4-nitrophenyl group interacted with Leu694 by *pi* interactions, and the (2, 3-dimethyl phenyl) amino moiety formed one H -bond with Asp831 (2.28 °A), while the benzamide moiety interacted with Cys773 by sulfur-*pi* interaction.

The 4*H*-1, 2, 4-triazole ring of compound HB5 created *pi* interaction with EGFR tyrosine kinase amino acid Leu694, while the (2,3-dimethyl phenyl) amino moiety formed *pi* interactions with Cys773 and Arg817, and the 4-nitrophenyl group interacted with Leu820, Ala719, Val702, and Lys721 by *pi* interactions, and one H- bond with Thr766 (2.33 °A).

Finally, the binding features of compound HB6 to essential amino acids of EGFR tyrosine kinase were mediated by 4*H*-1,2,4-triazole ring which demonstrated *pi* interactions with Leu820, Ala719, Leu694, and one H-bond with Met769 (2.44 °A), while the 4-methoxy phenylamino moiety formed *pi*-alkyl and *pi*-sulfur interactions with Ala719 and Cys751, respectively. The 4-nitrophenyl group formed *pi*-sigma interaction with Leu694, the (2, 3-dimethyl phenyl) amino moiety interacted with Cys773 by sulfur-*pi* interaction, and the benzamide moiety interacted with Asp831and Val702 by *pi*-anion and *pi*-alkyl interactions, respectively.

In silico ADMET and Drug likeness prediction

The ADMET properties of drugs are usually predicted by intestinal absorption, activity against colon cancer cell line (Caco-2), P-glycoprotein binding, and skin permeability levels (Han et al. 2019). The data displayed in Table 4 showed that among the tested compounds, HB1 had the best ADMET properties. Additionally, the results indicated the inability of all compounds to penetrate the blood-brain barrier (BBB), this in turn indicate that central nervous system (CNS) side effects are not expected

Table 4. ADMET properties for compounds HB1-HB6.

Properties	HB1	HB2	HB3	HB4	HB5	HB6	Erlotinib
Human gastrointestinal absorption	High	Low	Low	Low	Low	Low	High
Caco2	66.8	36.76	41.8	45.8	56.8	30.8	45.8
Bioavailability score	0.55	0.17	0.17	0.55	0.17	0.17	0.55
BBB penetration	NO	NO	NO	NO	NO	NO	Yes
PPB	95.35	80.46	81.30	91.69	84.36	89.39	75.69
CYP1A2 inhibitor	NO	NO	NO	NO	NO	NO	NO
CYP2C19 inhibitor	Yes	Yes	Yes	Yes	Yes	Yes	Yes
CYP2C9 inhibitor	NO	NO	NO	NO	NO	NO	NO
CYP2D6 inhibitor	NO	NO	NO	NO	NO	NO	NO
CYP3A4 inhibitor	Yes	Yes	Yes	Yes	Yes	Yes	Yes
Carcinogenicity	NO	NO	NO	NO	NO	mutant	NO
Ames Test	NO	NO	NO	NO	NO	NO	mutant

upon administration. The metabolism profile was predicted based on the CYP models, in particular (CYP1A2, CYP2C19, CYP2C9, CYP2D6, and CYP3A4), the results showed no inhibitory effect against most of the tested liver enzymes. Moreover, the toxicity of the tested compounds was predicted based on the AMES test, and the data displayed in Table 4 showed carcinogenicity profile of most derivatives close to zero.

The drug-likeness study indicated that all of the synthetic compounds (HB1-6) have most of Lipinski's Rule criteria for oral administration. In addition, it is known that for good bioavailability after oral administration the value of TPSA must not exceed 140 A°(Abbas et al. 2022), thus all tested compounds have good bioavailability, as shown in Table 5.

Table 5. Physicochemical properties of compounds (HB1– HB6).

Properties	HB1	HB2	HB3	HB4	HB5	HB6	Erlotinib
clog P	3.43	3.58	4.07	1.95	2.03	2.60	4.06
clog S	-10.83	-10.93	-11.41	-10.16	-10.25	-10.07	-7.26
H-bond acceptor	3	4	3	5	6	5	6
H-bond donor	3	3	3	3	3	3	1
Skin permeation (log Kp) cm/s	-4.19	-4.39	-3.95	-4.85	-4.79	-4.35	-6.35
TPSA (A°)	83.87	93.10	83.87	129.35	138.92	129.69	129.69

Table 6. *In*-vitro anti-proliferative activities of the tested compounds against Hep G2 and A549 cell lines. Data are presented as the mean of the IC_{50} values (μM) from three different experiments.

Compound	HepG2/IC_{50}	A549/IC_{50}
HB1	34.81	12.40
HB2	12.96	18.62
HB3	16.36	10.82
HB4	8.29	9.94
HB5	2.87	9.69
HB6	17.87	18.74

Biological study

The newly synthesized 1,2,4 triazole derivatives (HB1-6) are cytotoxic to cancer cells

The cytotoxic effects of the 6 compounds (HB1-HB6) were evaluated against Hep G2 and A549 human cancer cell lines using MTT assay (Suppl. material 1: Fig. S1). The IC_{50} values are shown in Table 6. The results revealed that all tested compounds exhibited cytotoxicity against Hep G2 hepatocyte carcinoma, and A549 lung cancer cell lines, 4 compounds (HB2, HB4, HB5, and HB6) were more cytotoxic to Hep G2 than to A459 cancer cells (lower IC_{50}; Table 6), while compounds HB1 and HB3 were more cytotoxic against A549 lung cancer cells. The lowest IC_{50} value achieved was with compound HB5 against Hep G2 hepatocyte carcinoma (2.87 μM; Table 6); thus, this compound was selected for further investigation at the IC_{50} concentration. The results of the MTT assay confirmed the superimposition results shown in Fig. 2, where the most cytotoxic compounds (HB5 and HB4) were the best superimposed (fittest) with erlotinib.

To study the selectivity of compound HB5 against cancer cells, the cytotoxicity of this compound was evaluated against the normal lung fibroblast cell line WI-38. The IC_{50} concentration of compound HB5 against WI-38 cells was 23.67 μM (Suppl. material 1: Fig. S1), resulting in a selectivity index (SI) of 8.25 (SI= IC_{50} normal cells/ IC_{50} cancer cells (Indrayanto et al. 2021). These data indicate that compound HB5 (molecular weight = 554.01 g/mol) exhibits strong cytotoxicity indicated by IC_{50} between 10 and 100 μg/mL (HB5 IC_{50}= 2.87 μM= 13.1 μg/mL), and high selectivity against cancer cells (SI ≥ 3) (Weerapreeyakul et al. 2012).

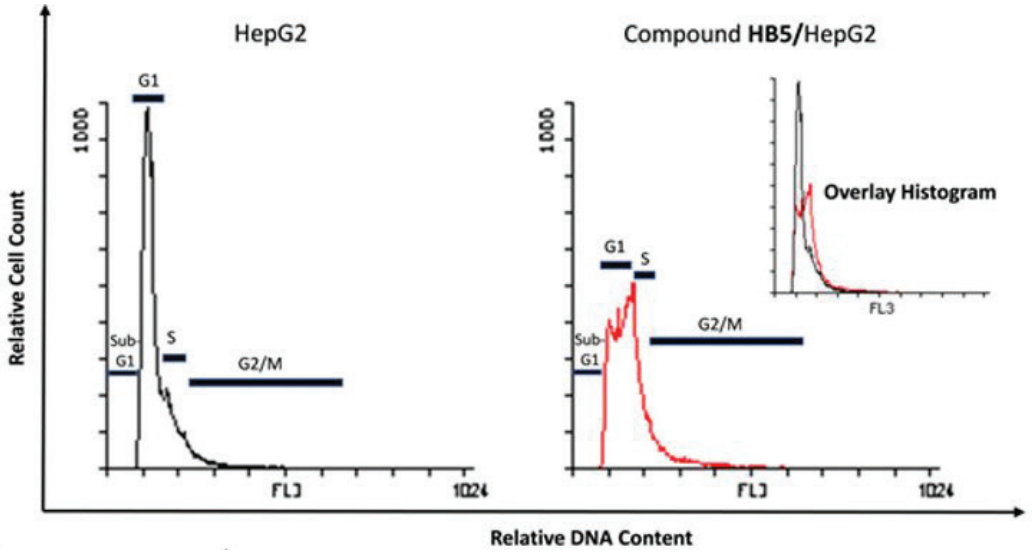

Figure 3. Flow cytometric analysis of Hep G2 cell cycle phases 48h-post compound HB5 treatment. Representative histograms showing the distribution of cell cycle phases of control and HB5-treated cells. Hep G2 hepatocyte carcinoma cells were treated with 2.87 μM (IC_{50} value) of compound HB5 for 48 h.

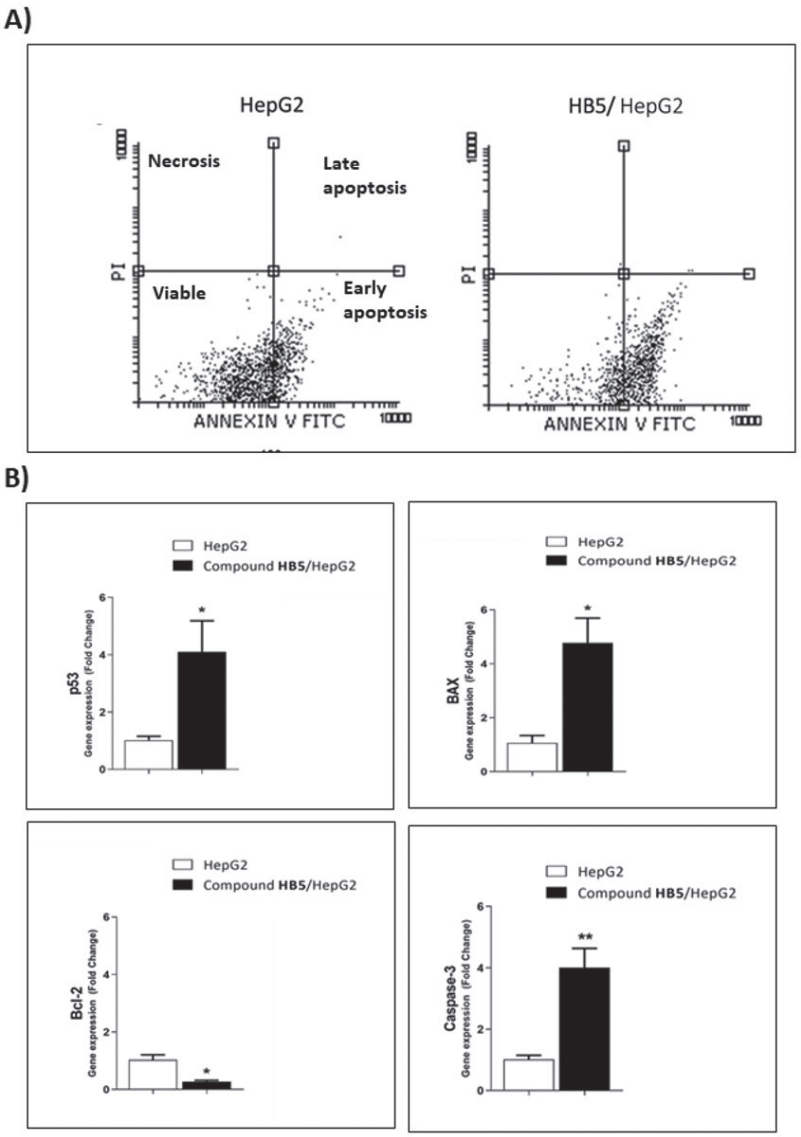

Figure 4. Treating Hep G2 hepatocyte carcinoma cells with compound HB5 induces apoptosis. **A** Representative flow cytometric charts for control and HB5-treated Hep G2 hepatocyte carcinoma cells showing the distribution of viable, apoptotic, and necrotic cells. Hep G2 cells were treated with compound HB5 (2.87 μM) for 48 h, fixed and stained with PI and fluorescent annexin V. Viable cells (bottom left; annexin V negative/PI negative), early apoptotic cells (bottom right; annexin V positive, PI negative), necrotic cells (top left; annexin V positive, PI positive), and late apoptotic cells (top right; annexin V positive, PI negative); **B** Total RNA was extracted from control and HB5-treated cells, reverse transcribed, and assayed for p53, BAX, Bcl-2, and caspase-3 gene expression by qRT-PCR. Data are presented as mean ± SEM of three independent experiments of the fold change in the ratio of relative mRNA levels of target gene/GAPDH (housekeeping gene). Fold change in control cells was set at 1 arbitrary unit. *$p < 0.05$, **$p < 0.01$ as compared to control cells.

Compound HB5-treated Hep G2 hepatocyte carcinoma cells are arrested at S and G2/M cell cycle phases

The effect of 48 h treatment of compound HB5 on Hep G2 cell cycle progression was evaluated by staining cells with PI followed by flow cytometry (Fig. 3). Data shown in Table 7 indicate that treating Hep G2 cells with the IC_{50} concentration of compound HB5 resulted in cell cycle arrest in the S and G2/M phases. The percentage of cells arrested in these phases increased by 50% when compared to control Hep G2 cells (Table 7).

Cytotoxicity of compound HB5 is attributed to apoptosis not necrosis

To investigate the mode of cell death (apoptosis versus necrosis) caused by 48h of compound HB5 treatment, Hep G2 cells were treated, stained with PI and annexin V-FITC, and analyzed by flow cytometry (Fig. 4A). As shown in Fig. 4A, Table 8, compound HB5 induced early apoptosis in treated cells as compared to control untreated cells.

Additionally, the level (fold change) of mRNA of apoptosis markers such as, p53, BAX (pro-apoptosis), Bcl-2 (anti-apoptosis), and caspase-3 was measured by qRT-PCR.

Table 7. Effect of compound HB5 on cell cycle progression in Hep G2 cells after 48 h treatment. Values are given as mean ± SEM of three independent experiments.

	Cell cycle distribution (%)			
	Sub-G1	G1	S	G2/M
Control Hep G2	0.63 ± 0.18	57.77 ± 2.68	25.35 ± 1.69	16.25 ± 1.34
HB5-treated Hep G2	1.16 ± 0.17	35.56 ± 5.08*	37.87 ± 3.87*	25.41 ± 2.18*

*p< 0.05 as compared to control cells.

Table 8. Effect of compound HB5 on the mode of cell death in Hep G2 cells after 48h treatment. Values are given as mean ± SEM of three independent experiments.

	% Viable	% Apoptosis		% Necrosis
		Early	Late	
Control Hep G2	93.55 ± 0.29	5.69 ± 0.30	0.62 ± 0.05	0.14 ± 0.03
HB5-treated Hep G2	28.21 ± 1.80****	70.44 ± 1.80****	1.21 ± 0.20	0.14 ± 0.01

****p< 0.0001 as compared to control cells.

The results shown in Fig. 4B indicate that the fold change of p53, BAX, and caspase-3 mRNA (normalized over GAPDH) increased, while the that of Bcl-2 mRNA decreased in HB5-treated Hep G2 cell line as compared to vehicle-treated control cells (set as 1 arbitrary unit) confirming induction of apoptosis in HB5-treated Hep G2 cells.

Compound HB5 inhibited Hep G2 cell proliferation and induced apoptosis by inhibiting EGFR tyrosine kinase

EGFR is one of the most frequently mutated genes in solid epithelial cancers, either through overexpression of the EGFR protein or a kinase-activating mutation (Sigismund et al. 2018b). In addition, the results of the molecular docking studies of compounds HB1-6 indicated that these compounds might be able to target EGFR tyrosine kinase. After analyzing the results of the EGFR kinase inhibition assay, it was found that compound HB5 exhibited inhibitory activity against EGFR tyrosine kinase (EC_{50}= 38.3 nM), which was comparable to the EC_{50} concentration of the standard chemotherapeutic drug erlotinib (EC_{50}= 9.6 nM) (Suppl. material 2: Fig. S2).

All tested compounds have the same pattern of pharmacophoric queries of EGFR tyrosine kinase inhibitors, however, compound HB5 has the highest fitting with these queries. Compound HB5 showed

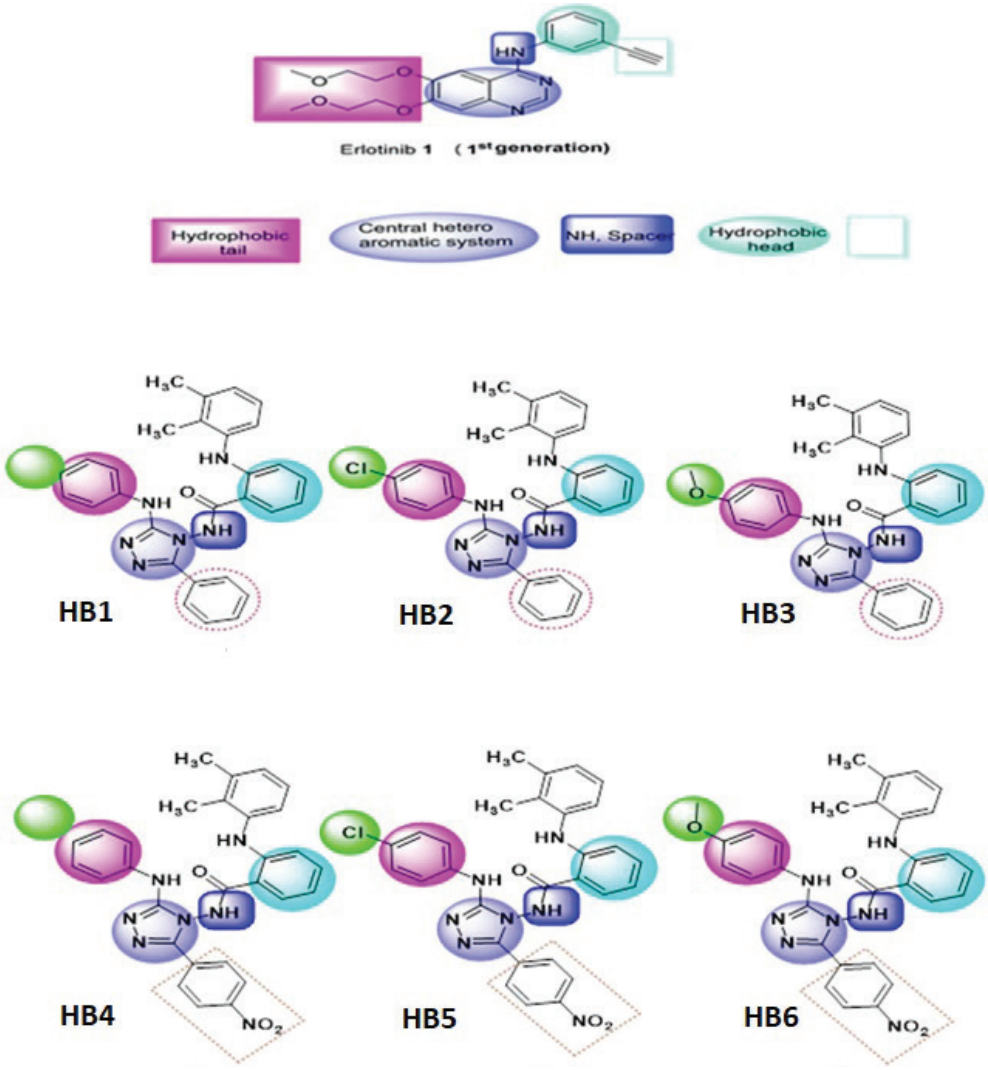

Figure 5. The synthesized compounds predicted feature as EGFR tyrosine kinase inhibitors.

the lowest ΔG score (-8.32 Kcal/mol; Table 3) in the interaction with EGFR tyrosine kinase, which indicates the stability of interaction between HB5 and the "Hit" amino acids in the target site of EGFR tyrosine kinase. This in turn indicates high selectivity and activity against the EGFR tyrosine kinase target site, confirmed by docking studies and superimposition as well as the EGFR inhibitory assay, which explains the ability of compound HB5 to cause the strongest cytotoxicity, i.e., lowest IC_{50} value (Table 6).

Structure-Activity Relationship (SAR) of compounds HB1-HB6

The SAR of the compounds (HB1-6) revealed several common findings (Fig. 5). For anti-cancer activity, the fragment binding to the hydrophilic linker is essential to be an aryl or heteroaryl (Gaber et al. 2021). Accordingly, the compounds which have 4-nitrophenyl moiety (compounds HB4, HB5, and HB6) showed good activity nearly equal with those compounds containing 4-phenyl moiety (compounds HB1, HB2, and HB3). Additionally, compounds that contain chloro (Cl) groups in hydrophobic tail, showed the best activity against targeted cells according to the MTT assay (compounds HB2 and HB5), moreover, the 4-nitrophenyl ring attached to central aromatic is more preferable than non-derivatization. Thus, for the tested compounds (HB1- HB6), chloro derivative in the hydrophobic tail (HB5) is better than methoxy(HB6), and phenyl derivative (HB4).

Conclusion

A series of 1,2,4 triazole derivatives (HB1-6) have been successfully synthesized, and their chemical structures were confirmed using FT-IR, ^{1}H, and $^{13}CNMR$ spectra and elemental microanalysis. After performing molecular docking studies and MTT assay for the tested compounds, the results showed a high correlation between the expected results from the molecular modeling and the wet-lab biological evaluations, which indicated high selectivity against the EGFR tyrosine kinase target site. Additionally, *in* silico *pre*-ADMET study showed that all tested compounds have no CNS side effects, and carcinogenicity score close to zero. Finally, compound HB5 showed the strongest cytotoxicity and highest selectivity against cancer cells through its stable interaction with EGFR tyrosine kinase leading to inhibition of its activating, and thus inducing cancer cell apoptosis.

Conflict of Interest

The authors declare that there is no conflict of interest.

Acknowledgements

The authors are grateful to Department of Pharmaceutical Chemistry, College of Pharmacy, University of Basrah, Iraq, for supporting the current work.

References

Abbas SQ, Ali F, Ishaq M, Bano I, Hassan M, Jin H-Z, Bungau SG (2022) A Comprehensive in silico exploration of pharmacological properties, bioactivities, molecular docking, and anticancer potential of vieloplain F from Xylopia vielana Targeting B-Raf Kinase. Molecules 27(3): e917. https://doi.org/10.3390/molecules27030917

Al-Bayati AI, Mahmood AAR, Al-Mazaydeh ZA, Rammaha MS, Al-Bayati RI, Alsoubani F, Tahtamouni LH (2021a) Synthesis, docking study, and in vitro anticancer evaluation of new flufenamic acid derivatives. Pharmacia 68: 449–461. https://doi.org/10.3897/pharmacia.68.e66788

Al-Bayati AI, Mahmood AAR, Tahtamouni LH, Al-Mazaydeh ZA, Rammaha MS, Al-Bayati RI, Alsoubani F (2021b) Synthesis, docking study, and in-vitro anti-cancer evaluation of new triazole derivatives of flufenamic acid. Materials Today: Proceedings. https://doi.org/10.1016/j.matpr.2021.05.317

Al-Saad HN, Mahmood AAR, Al-Bayati RI (2019) Design, synthesis, docking study and antiplatelet evaluation of new thiosemicarbazide derivatives derived from Captopril. Oriental journal of chemistry 35(2): 829–838. http://doi.org/10.13005/ojc/350246

Arienti C, Pignatta S, Tesei A (2019) Epidermal growth factor receptor family and its role in gastric cancer. Frontiers in Oncology 9: 1–11. https://doi.org/10.3389/fonc.2019.01308

Belli S, Esposito D, Servetto A, Pesapane A, Formisano L, Bianco R (2020) c-Src and EGFR inhibition in molecular cancer therapy: what else can we improve? Cancers 12: 1489–1505. https://doi.org/10.3390/cancers12061489

Chopra N, Kaur D, Chopra G (2018) Nature and hierarchy of hydrogen-bonding interactions in binary complexes of azoles with water and hydrogen peroxide. ACS omega 3(10): 12688–12702. https://doi.org/10.1021/acsomega.8b01523

Chu XM, Wang C, Wang WL, Liang LL, Liu W, Gong KK, Sun KL (2019) Triazole derivatives and their antiplasmodial and antimalarial activities. European Journal of Medicinal Chemistry 166: 206–223. https://doi.org/10.1016/j.ejmech.2019.01.047

Das M, Das B, Samanta A (2019) Antioxidant and anticancer activity of synthesized 4-amino-5-((aryl substituted)-4H-1,2,4-triazole-3-yl) thio-linked hydroxamic acid derivatives. Journal of Pharmacy and Pharmacology 71: 1400–1411. https://doi.org/10.1111/jphp.13131

Debela DT, Muzazu SG, Heraro KD, Ndalama MT, Mesele BW, Haile DC, Kitui SK, Manyazewal T (2021) New approaches and procedures for cancer treatment: Current perspectives. SAGE open medicine 9: 1–11. https://doi.org/10.1177/20503121211034366

El-Sebaey S (2020) Recent Advances in 1, 2, 4-Triazole Scaffolds as Antiviral Agents. ChemistrySelect 5: 11654–11680. https://doi.org/10.1002/slct.202002830

Fattah HAA (2014) Synthesis, cytotoxic and antimicrobial activities of novel 1,2,4- triazole derivatives incorporating aryl sulfonamide moiety. Chemistry 22: 190–201.

Gaber AA, El-Morsy AM, Sherbiny FF, Bayoumi AH, El-Gamal KM, El-Adl K, Al-Karmalawy AA, Ezz Eldin RR, Saleh MA, Abulkhair HS (2021) Pharmacophore-linked pyrazolo [3, 4-d] pyrimidines

as EGFR-TK inhibitors: Synthesis, anticancer evaluation, pharmacokinetics, and in silico mechanistic studies. Archiv der Pharmazie, e2100258. https://doi.org/10.1002/ardp.202100258

Grytsai O, Valiashko O, Penco-Campillo M, Dufies M, Hagege A, Demange L, Martial S, Pagès G, Ronco C, Benhida R (2020) Synthesis and biological evaluation of 3-amino-1,2,4-triazole derivatives as potential anticancer compounds. Bioorganic Chemistry 104: 1–20. https://doi.org/10.1016/j.bioorg.2020.104271

Gurdal H, Tuglu MM, Bostanabad SY, Dalkiliç B (2019) Partial agonistic effect of cetuximab on epidermal growth factor receptor and Src kinase activation in triple-negative breast cancer cell lines. International Journal of Oncology 54: 1345–1356. https://doi.org/10.3892/ijo.2019.4697

Han Y, Zhang J, Hu CQ, Zhang X, Ma B, Zhang P (2019) In silico ADME and toxicity prediction of ceftazidime and its impurities. Frontiers in Pharmacology 10: 434–434. https://doi.org/10.3389/fphar.2019.00434

Iacopetta D, Lappano R, Mariconda A, Ceramella J, Sinicropi MS, Saturnino C, Talia M, Cirillo F, Martinelli F, Puoci F (2020) Newly synthesized imino-derivatives analogues of resveratrol exert inhibitory effects in breast tumor cells. International Journal of Molecular Sciences 21: 1–17. https://doi.org/10.3390/ijms21207797

Indrayanto G, Putra GS, Suhud F (2021) Validation of in-vitro bioassay methods: Application in herbal drug research. Profiles of Drug Substances, Excipients, and Related Methodology 46: 273–307. https://doi.org/10.1016/bs.podrm.2020.07.005

Jiang X, Liu Y, Zhang G, Lin S, Wu J, Yan X, Ma Y, Ma M (2020) Aloe-Emodin induces breast tumor cell apoptosis through Upregulation of miR-15a/miR-16-1 That Suppresses BCL2. Evidence-Based Complementary and Alternative Medicine 2020: e5108298. [10 pp] https://doi.org/10.1155/2020/5108298

Kaur R, Dwivedi AR, Kumar B, Kumar V (2016) Recent developments on 1,2,4-triazole nucleus in anticancer compounds: A review. Anti-cancer agents in Medicinal Chemistry16(4): 465–489. https://doi.org/10.2174/1871520615666150819121106

Kazberuk A, Zareba I, Palka J, Surazynski A (2020) A novel plausible mechanism of NSAIDs-induced apoptosis in cancer cells: the implication of proline oxidase and peroxisome proliferator-activated receptor. Pharmacological Reports 72: 1152–1160. https://doi.org/10.1007/s43440-020-00140-z

Kerru N, Gummidi L, Maddila S, Gangu KK, Jonnalagadda SB (2020) A review on recent advances in nitrogen-containing molecules and their biological applications. Molecules 25(8): 1–42. https://doi.org/10.3390/molecules25081909

Khodapasand E, Jafarzadeh N, Farrokhi F, Kamalidehghan B, Houshmand M (2015) Is Bax/Bcl-2 ratio considered as a prognostic marker with age and tumor location in colorectal cancer? Iranian biomedical journal 19: 69–75.

Krishna R, Sridhar G, Jayaprakash HV (2020) Synthesis and anticancer activity of novel 1,2,3-Triazole ring incorporated 1,2,4-Oxadiazole-1,3-Oxazole Derivatives. Russian Journal of General Chemistry 90: 901–906. https://doi.org/10.1134/S1070363220050242

Kuntala N, Mareddy J, Telu JR, Banothu V, Pal S, Anireddy JS (2021) Non-steroidal anti-inflammatory drugs based new 1, 2, 3-triazole derivatives: their design, one-pot synthesis and in vitro evaluation. Journal of Heterocyclic Chemistry 58: 2018–2032. https://doi.org/10.1002/jhet.4328

Lakkakula R, Roy A, Mukkanti K, Sridhar G (2019) Synthesis and anticancer activity of 1,2,3-triazole fused N-arylpyrazole derivatives. Russian Journal of General Chemistry 89: 831–835. https://doi.org/10.1134/S1070363219040315

Liu Z, Ning F, Cai Y, Sheng H, Zheng R, Yin X, Lu Z, Su L, Chen X, Zeng C (2021) The EGFR-P38 MAPK axis up-regulates PD-L1 through miR-675-5p and down-regulates HLA-ABC via hexokinase-2 in hepatocellular carcinoma cells. Cancer communications 41: 62–78. https://doi.org/10.1002/cac2.12117

Maennling AE, Tur MK, Niebert M, Klockenbring T, Zeppernick F, Gattenlöhner S, Meinhold-Heerlein I, Hussain AF (2019) Molecular targeting therapy against EGFR family in breast cancer: Progress and future potentials. Cancers 11(12): 1–19. https://doi.org/10.3390/cancers11121826

Mahdi MF, Alsaad HN (2012) Design, synthesis and hydrolytic behavior of mutual prodrugs of NSAIDs with gabapentin using glycol spacers. Pharmaceuticals 5: 1080–1091. https://doi.org/10.3390/ph5101080

Nunez R (2001) DNA measurement and cell cycle analysis by flow cytometry. Current Issues in Molecular Biology 3: 67–70.

Peluffo MC, Young KA, Stouffer RL (2005) Dynamic expression of caspase-2, -3, -8, and -9 proteins and enzyme activity, but not messenger ribonucleic acid, in the monkey corpus luteum during the menstrual cycle. Journal of Clinical Endocrinology and Metabolism 90: 2327–2335. https://doi.org/10.1210/jc.2004-2214

Peyton L, Gallagher S, Hashemzadeh M (2015) Triazole antifungals: A review. Drugs of today 51: 705–718.

Pozarowski P, Darzynkiewicz Z (2004) Analysis of cell cycle by flow cytometry. Methods in Molecular Biology 281: 301–311. https://doi.org/10.1385/1-59259-811-0:301

Shabeeb I, Al-Essa L, Shtaiwi M, Al-Shalabi E, Younes E, Okasha R, Abu Sini M (2019) New hydrazide-hydrazone derivatives of quinoline 3-carboxylic acid hydrazide: synthesis, theoretical modeling and antibacterial evaluation. Letters in Organic Chemistry 16: 430–436. https://doi.org/10.2174/1570178616666181227122326

Shaikh MH, Subhedar DD, Nawale L, Sarkar D, Khan FAK, Sangshetti JN, Shingate BB (2019) Novel benzylidenehydrazide-1,2,3-triazole conjugates as antitubercular agents: Synthesis and molecular docking. Mini-Reviews in Medicinal Chemistry 19: 1178–1194. https://doi.org/10.2174/1389557518666180718124858

Sigismund S, Avanzato D, Lanzetti L (2018a) Emerging functions of the EGFR in cancer. Molecular oncology 12: 3–20. https://doi.org/10.1002/1878-0261.12155

Sigismund S, Avanzato D, Lanzetti L (2018b) Emerging functions of the EGFR in cancer. Molecular oncology12: 3–20. https://doi.org/10.1002/1878-0261.12155

Weerapreeyakul N, Nonpunya A, Barusrux S, Thitimetharoch T, Sripanidkulchai B (2012) Evaluation of the anticancer potential of six herbs against a hepatoma cell line. Chinese medicine 7: 15–15. https://doi.org/10.1186/1749-8546-7-15

Woo DH, Han IS, Jung G (2004) Mefenamic acid-induced apoptosis in human liver cancer cell-lines through caspase-3 pathway. Life Sciences 75: 2439–2449. https://doi.org/10.1016/j.lfs.2004.04.042

World Health Organization (2020) Health topics. WHO, Geneva. https://www.who.int/health-topics/cancer#tab=tab_1

Zhang X, Wang Q, Xu Y, Wang B, Jia C, Wang L, Sun H, Zhao H, Wang Z, Zou Q, Sun S, Zhang L (2019) lncRNA PCAT19 negatively regulates p53 in non-small cell lung cancer. Oncology Letters 18: 6795–6800. https://doi.org/10.3892/ol.2019.11041

Zhang Y, Liu X, Lin Y, Lian B, Lan W, Iovanna JL, Liu X, Peng L, Xia YJCC (2020) Novel triazole nucleoside analogues promote anticancer activity via both apoptosis and autophagy. Chemical Communications, Royal Society of Chemistry 56: 10014–10017. https://doi.org/10.1039/D0CC04660D

Supplementary material 1

Figure S1

Authors: Hiba Alsaad, Ammar Kubba, Lubna H. Tahtamouni, Ali H. Hamzah

Data type: JPG file

Explanation note: HB5-treated Hep G2 hepatocyte carcinoma and A549 lung cancer cells show reduced cell proliferation. Representative line chart of the MTT assay results. Cells were treated for 48h and the growth inhibition percentage (Inhibition %) relative to the vehicle-treated control cells was measured. Percent inhibition was calculated according to the following formula: optical density (OD) treated/OD vehicle-treated control×100%. The experiment was performed three times in triplicates.

Link: https://doi.org/10.3897/pharmacia.69.e83158.suppl1

Supplementary material 2

Figure S2

Authors: Hiba Alsaad, Ammar Kubba, Lubna H. Tahtamouni, Ali H. Hamzah

Data type: JPG file

Explanation note: The EGFR tyrosine kinase inhibitory activity of compound HB5 was comparable to that of erlotinib. The inhibitory activities of compound HB5 and erlotinib (a standard TKI) against EGFR kinase were evaluated by chemiluminescence and the EC50 values were determined in nM.

Link: https://doi.org/10.3897/pharmacia.69.e83158.suppl2